Thickness of sediments in the Congo basin based on the analysis of decompensative gravity anomalies

Mikhail K. Kaban [a,b,*], Damien Delvaux [c], Francesca Maddaloni [d], Magdala Tesauro [d,e], Carla Braitenberg [d], Alexey G. Petrunin [a,b], Sami El Khrepy [f,g]

[a] Helmholtz-Centre Potsdam - GFZ German Research Centre for Geosciences, Telegrafenberg A20, D-14473, Potsdam, Germany
[b] Schmidt Institute of Physics of the Earth, Moscow, Russia
[c] Royal Museum of Central Africa, Tervuren, Belgium
[d] Dept. of Mathematics and Geosciences, University of Trieste, Trieste, Italy
[e] Dept. Earth Sciences, University of Utrecht, Utrecht, Netherlands
[f] King Saud University, Riyadh, Saudi Arabia, P.O. Box 2455, Riyadh, 11451, Saudi Arabia
[g] National Research Institute of Astronomy and Geophysics, NRIAG, 11421, Helwan, Egypt

ARTICLE INFO

ABSTRACT

The Congo basin is one of the largest intracratonic basins in the World, locating within a cold lithospheric plate. The structure of the thick sedimentary layer is investigated by seismic studies only in limited places. Here, we present a map of sedimentary thickness for the whole Congo basin, based on the inversion of the decompensative gravity anomalies. Contrary to the conventional Bouguer or isostatic gravity anomalies, the effect of the isostatic compensation of sediments is reduced in the decompensative anomalies, which provides a possibility to recover the full effect of low-density sediments. The calculated decompensative correction reaches ±70 mGal and exceeds the amplitude of the isostatic anomalies, especially in the long wavelengths. The final decompensative anomalies are negative over the whole basin and their patterns well correspond to its tectonic fragmentation. By inverting these anomalies with the predefined density-depth relationship we have obtained the sedimentary thickness map for the whole Congo basin. The maximum basement depth exceeding 10 km is found in the Lokoro basin and basins in the South. In the Lomami basin, thickness of sediments reaches about 6.5 km. It is important to note, that these deep depressions, are not covered by seismic studies. Furthermore, we found a new deep basin adjacent to the Lokonia High (on the SW side) that we propose to name as the Salonga basin.

1. Introduction

The Congo basin (CB), known as Cuvette Centrale (Fig. 1), is one of the largest intracratonic basins in the World, covering large part (1.4 × 10^6 km^2) of the Congo craton, an amalgamation of crustal blocks of Archean and Proterozoic age (Kadima et al., 2011a). The formation of the CB started with a rifting phase during the amalgamation of the Rodinia supercontinent at about 1.1 Gyr ago and the main episodes of subsidence occurred during the following post-rift phase in the Late Proterozoic (De Wit et al., 2008; Kadima et al., 2011a, b; Delvaux et al., 2021). Minor phases of subsidence and uplift affected the CB during the Paleozoic, as a consequence of the Pan-African deformation and from the far-field effects of the Gondwanides orogeny at the north-western margin of the Gondwana continent (Daly et al., 1991; Trouw and De Wit, 1999). Since the Cretaceous, the CB has been subjected to an intraplate compressional setting due to ridge-push forces related to the spreading of the South Atlantic Ocean (Delvaux and Barth, 2010) and since Oligocene, to the influence of the East African Rift (Macgregor, 2015). The resulting uplift phases caused the erosion of most of sediments, while sedimentation was limited to the center of the basin (Kadima et al., 2011a). Existing seismic reflection and refraction profiles provide the total thickness of sediments up to 9 km and probably more in some places (ECL, 1988; Lawrence and Makazu, 1988; Daly et al., 1992).

The CB, which is located between the Atlantic coast and the Western branch of the East African Rift System (EARS) is considered of moderate seismicity (Fig. 2), which could be related to its subsurface structures beneath Cretaceous to Cenozoic sediments (Daly et al., 1992). Therefore, knowledge of the sedimentary structure is also important for
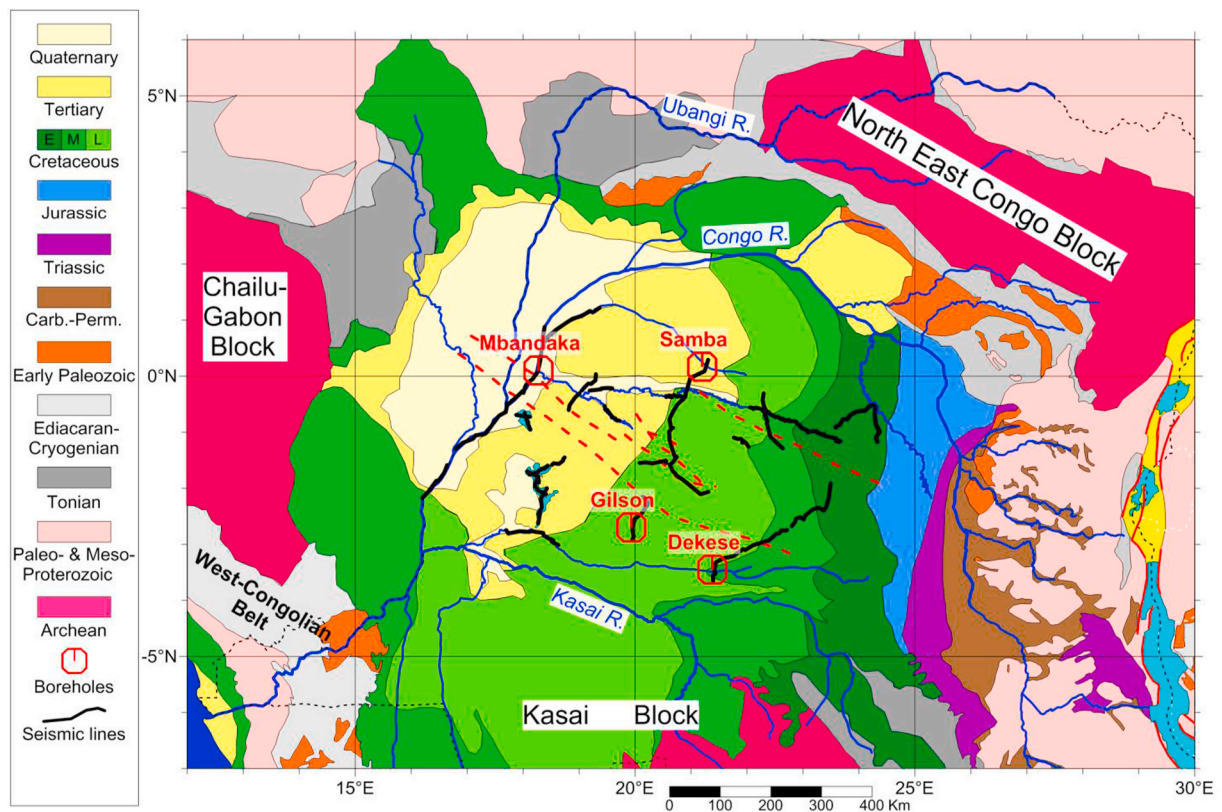

Fig. 1. Geological map of the Congo basin and surroundings. Red octagons identified by names show locations of four boreholes.
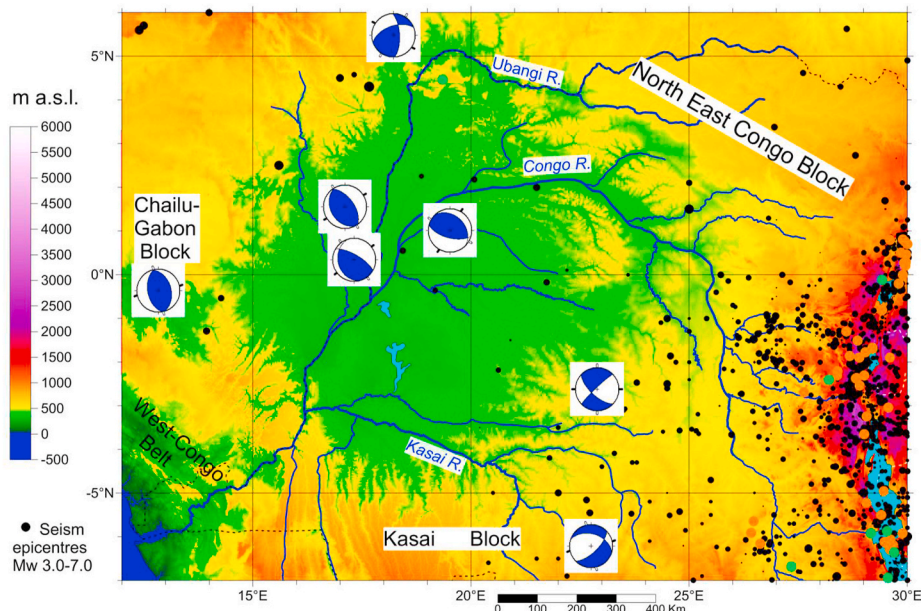

Fig. 2. Topography of the Congo Basin and surroundings (Becker et al., 2009) and epicenters of earthquakes (ISC-GEM, Storchak et al., 2013). The Congo Basin is limited to the east by the western branch of the East African Rift (visible are from N to S: lakes Edouard, Kivu and Tanganyika). The focal mechanisms are from Delvaux and Barth (2010).

understanding the seismicity distribution. Since the CB is located close to the boarder of the East African Swell and the EARS, it is directly affected by active tectonics of these structures. Some areas in the CB have been subjected to damaging earthquakes of shallow crustal depths and Mb = 5.4–5.6 in the period 1976–1998 (Fairhead and Stuart, 1982). The fault plane solutions of these earthquakes indicate thrust faulting and horizontal compression with P-axes chiefly aligned E-W (Ayele, 2002; Downey and Gurnis, 2009). Delvaux and Barth (2010) have found pure thrust faulting for seven events and minor strike slip and normal faulting for one event solutions in the CB. Craig et al. (2011) suggested that the distribution of the thrust faults and related earthquakes is probably due to the dynamically induced stresses.
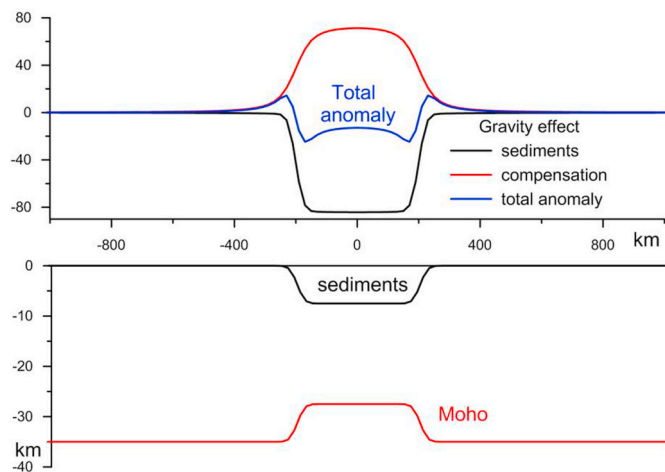
Fig. 3. Synthetic example of the total gravity effect of the sedimentary basin (isostatic anomalies) that is compensated by the Moho variations.

The CB is located over a cold lithospheric block with a thickness of about 200 km and requires a deep compensation level to explain the underlying long-wavelength negative gravity anomaly, one of the largest on the Earth (e.g., Downey and Gurnis, 2009; Buiter et al., 2012). This anomaly is thought as the result of the combination of the effects of the low density of its thick sedimentary units and the presence of a high-density body below the crust, which isostatically compensates the sediments (e.g. Hartley and Allen, 1994). Other studies link the subsidence of the basin to tectonic uplift of swells surrounding the basin (Burke and Gunnell, 2008) or to lithospheric delamination (Downey and Gurnis, 2009).

Existing maps of sediments covering the whole CB (e.g. Crosby et al., 2010) are usually based on the models CRUST2.0 and CRUST1.0 (Laske and Masters, 2013), which in turn represent digitized thickness of sediments from the "Tectonic Map of the World" (Exxon, 1985). The last one is outdated and does not fit to existing seismic determinations. Geophysical campaigns carried out in the CB between 1974 and 1976 acquired about 2900 km of seismic reflection profiles (e.g. Daly et al., 1992; Kadima et al., 2011a). Their recent interpretation provides good constraints on the sedimentary structure of the central part of the CB (Kadima et al., 2011a; Maddaloni et al., 2019; Delvaux et al., 2021). However, the results of the interpolation of the seismic data have to be validated, while other parts of the CB remain uncovered by data. Recent satellite missions combined with existing terrestrial and airborne observations provided for the first time homogeneous high-resolution models of the gravity field (e.g. Förste et al., 2014). This field can be used to study structure of the crust and lithosphere, as demonstrated by many studies. Several studies using gravity data aimed to investigate the structure of the lithosphere of the CB have been performed (e.g. Ebbing et al., 2007; Crosby et al., 2010; Kadima et al., 2011b; Buiter et al., 2012). All authors found a regional minimum coinciding with the CB with an amplitude of about (30–40 mGal). They related this minimum to the upper mantle structure and dynamics (e.g., Crosby et al., 2010) or to the effect of sediments (e.g., Buiter et al., 2012). Kadima et al. (2011b) pointed that the gravity field over the CB with surrounding area reflect several trends (local and regional), which are difficult to separate. They also found evidence for the presence of salt within the basin, influencing the tectonic deformations. However, the total negative anomaly is too small to be explained solely by the effect of thick sediments.

Usually, for investigation of the upper crust density structure, the calculation of the isostatic anomalies of the gravity field are considered as most appropriate. The effect of deep density variations (e.g. of the Moho) is eliminated from the observed field with the isostatic correction (e.g. Blakely 1995; Simpson et al., 1986; Watts, 2001), and recently by machine learning techniques analyzing gravity and topography (Pivetta

and Braitenberg, 2020). This approach is mostly used, when a few or no data constrain the deep density structure of the crust and upper mantle. It has been demonstrated that the results chiefly depend on the integrated parameters of the isostatic compensation model, i.e. the average compensation depth (predominantly determined by the Moho boundary) and effective elastic thickness of the lithosphere, which can be determined a-priory. Consequently, the isostatic anomalies were used in many studies to determine the structure of sedimentary basins around the World (e.g. Jachens and Moring, 1990; Langenheim and Jachens, 1996; Ebbing et al., 2007).

However, the isostatic gravity anomalies do not show a complete effect of sediments or other upper crust density heterogeneity, since they are compensated in isostatic sense (locally or regionally) and their gravity influence is largely diminished by the opposing effect of the compensating masses, especially for horizontally extended structures (Cordell et al., 1991). A synthetic example of the total effect of sediments and their compensation is shown in Fig. 3. The pure effect of sediments is about −70 mGal, but it is reduced to about −10 mGal in the central part of the 400 km wide basin, due to the effect of the isostatic compensation at the Moho. Only substantial edge effects are left at the flanks of the basin. For the CB, which is at least two times wider, the reduction would be even much more significant.

The pure gravity effect of sediments can be restored by applying a decompensative correction suggested by Zorin et al. (1985) and Cordell et al. (1991). The resulting decompensative gravity anomalies can be successfully employed then for studying the upper crust, including sediments, as was demonstrated in previous studies of different areas (Hildenbrand et al., 1996; Cordell et al., 1991; Wilson et al., 2005; Zorin et al., 1993). In these studies, only a local isostatic model was considered, which imposed serious limitations on the obtained results. Recently, this method has been extended to the case of regional isostatic compensation and employed for studying the Middle East and Antarctica (Kaban et al., 2017; Haeger and Kaban, 2019).

In the present study, we calculate the decompensative gravity anomalies for the CB and surrounding areas and interpret them with respect to the thickness of sediments. The results are analysed in connection with the tectonic structure of the region.

2. Decompensative gravity anomalies

2.1. Isostatic and decompensative corrections of the gravity field

The isostatic anomalies represent the residual gravity field obtained after removing the effects of topography/bathymetry and their compensation according to an adopted model of the isostatic compensation from the observed anomalies (Blakely, 1995). In this way, it is possible to refine the Bouguer gravity anomalies from the effect of deep masses, which is highly correlated with the observed topography/bathymetry and related to deep density heterogeneity. Therefore, the residual isostatic anomalies are largely related to the upper crust. This approach is very useful when only a little is known about structure of the crystalline crust and upper mantle. It has been demonstrated that the most important parameters of the compensation scheme are the compensation depth and effective elastic thickness of the lithosphere (EET) (e.g. Forsyth, 1985). The compensation depth is mainly related to the average position of the Moho, which is known with sufficient accuracy when we do not consider local variations. EET can be also determined independently (e.g., Kadima et al., 2011b; Tesauro et al., 2012). The EET values may vary in details depending on method used to evaluate it, however the general trends associated with the high EET over the Congo craton are clearly consistent. Possible differences can only affect very long wavelengths, which are not considered in this study.

In the spectral domain, the isostatic correction can be formulated as the following (Kaban et al., 2016):
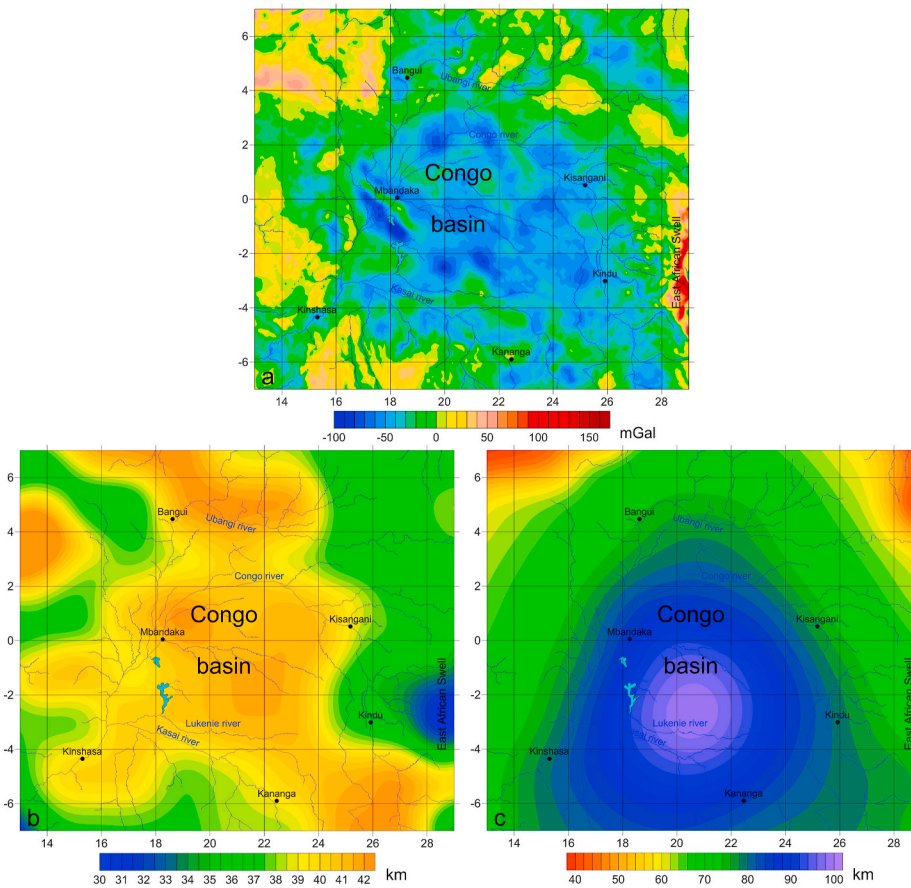
Fig. 4. Initial data. (a) Free air gravity anomalies (disturbances, Förste et al., 2014); (b) Depth to the Moho (Laske and Masters, 2013); (c) Effective elastic thickness of the lithosphere (Tesauro et al., 2012).

$$\Delta g_{ic}\ (k_x, k_y)\ =\ G_{is}(k_x, k_y) \cdot t_{adj}(k_x, k_y)$$
$$=\ -2\pi G\rho\ \ C \cdot \exp(-k \cdot M)\ \cdot\ t_{adj}(k_x, k_y) \quad (1)$$

where $k = \sqrt{k_x^2 + k_y^2}$ is the wavenumber, $k_x = 2\pi/\lambda_x$ and $k_y = 2\pi/\lambda_y$, G is the gravitational constant, M is the depth to the Moho, which is associated with the isostatic compensation depth, t_{adj} is the adjusted topography, which is introduced in the sea area to equalize the bathymetry (t_b) and topography variations for the constant density of the topography ρ:

$$t_{adj} = t_b - \frac{\rho_w}{\rho} t_b, \quad (2)$$

where $\rho_w = 1.03$ g/cm^3 is the water density. For the study area, the adjusted topography is equivalent to the "normal" topography, the correction is applied in the sea area, which data are used to estimate far-field effects.

The parameter C depends on the wavenumber and EET (T_e) (e.g. Turcotte and Schubert, 1982):

$$C\ =\ \Delta\rho g / (k^4 D + \Delta\rho g), \quad (3)$$

where $D = ET_e^3 / [12(1 - \nu^2)]$ is the flexural rigidity of the lithosphere, E is the Young modulus, ν is the Poisson ratio, $\Delta\rho$ is the average difference of the density of topography and the upper mantle material, and g is the gravitational acceleration. This parameter characterizes the amount of the isostatic compensation (C = 1 for the local Airy isostatic model).

It is difficult to use Eq. (2) directly for calculation of the isostatic correction in the spectral domain with horizontally varying EET. We employ a convolution of the adjusted topography with corresponding

Green's functions that depend on the average Moho depth and EET, following the approach of Wienecke and Braitenberg (2007), Braitenberg et al. (2002) and Dill et al. (2015). These authors have demonstrated that this approach is sufficiently accurate for modelling the response of the lithosphere to the external load. The isostatic anomalies (Δg_i) are computed as follows:

$$\Delta g_i(x_0, y_0) = \Delta g_b(x_0, y_0) + \iint_{-1250km}^{1250km} t_{adj}(x_0 + x, y_0 + y) \cdot G_{is}(x, y, M, T_e) dx dy$$
$$G_{is}(x, y, M, T_e) = F^{-1}\big(G_{is}(k_x, k_y, M, T_e)\big) \quad (4)$$

where G_{is} is the Green's function, F^{-1} is the inverse Fourier transform, and $\Delta g_b(x, y)$ stands for the Bouguer gravity anomalies.

The residual isostatic anomalies are yet influenced by the dynamic effects of the mantle convection and glacial isostatic adjustments. However, their effects appear at the long-wavelengths (>2500 km, Kaban et al., 1999, 2004), while the anomalies related to the upper crust are limited by their horizontal dimension (up to 1000 km for the CB) and maximum value of EET (~70 km, e.g. Tesauro et al., 2012). Therefore, a Gauss type filter on the sphere with the boundary wavelength (half amplitude) 2500 km was applied to remove the dynamic effects from the isostatic anomalies (Kaban et al., 1999). It is also important that the boundary wavelength 2500 does not reduce the decompensative correction for the whole Congo basin, whose size approximately corresponds to the half-wavelength (1250 km). It is clear that the effect of sub-crustal density inhomogeneities extends to shorter wavelengths. However, this effect is largely considered when calculating the isostatic and decompensative gravity anomalies, although it is assumed in the simplified expressions that the whole compensation occurs at the Moho
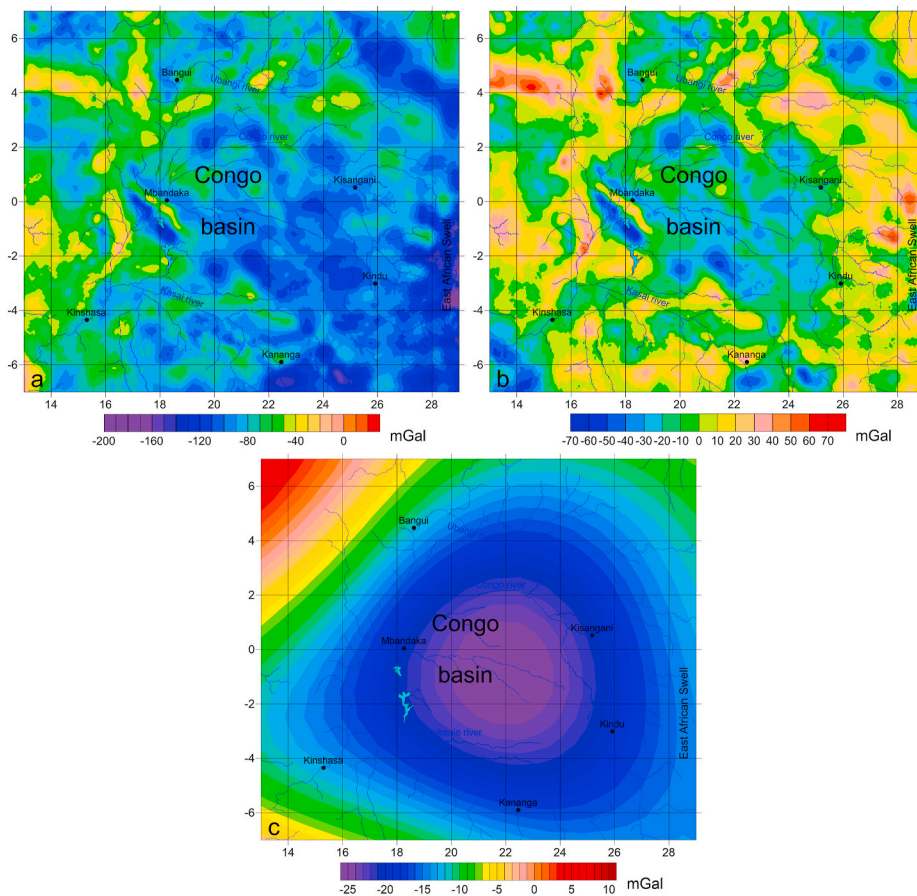
Fig. 5. Bouguer (a) and residual isostatic (b) gravity anomalies. (c) Long-wavelength part of the full isostatic anomalies, which has been removed.

depth. In reality, it is also provided by crystalline crust and upper mantle density variations, but these depth changes only marginally affect the result.

The decompensative correction (Δg_{dc}) is formulated as follows (Kaban et al., 2017):

$$\Delta g_{dc}\ (k_x, k_y)\ =\ \frac{1}{\exp(k \cdot M)/C\ -\ 1} \Delta g_i (k_x, k_y)\ ,\ . \tag{5}$$

where Δg_i are the isostatic anomalies, other terms are as in Eqs. (1)–(3). This equation is based on formulations of Zorin et al. (1985) and Cordell et al. (1991), which are improved for the case of elastic support (Kaban et al., 2017). This correction exponentially increases with wavelength approaching infinity, therefore Cordell et al. (1991) suggested to apply a high-pass filter to reduce it above some boundary wavelength (λ_0). Although the long-wavelength component is already removed from the residual isostatic anomalies, the decompensative correction might be overestimated anyway as demonstrated by Kaban et al. (2017). Therefore, a high-pass filter starting from the wavelength 2500 km (the same as for the isostatic anomalies) with a gradual decrease for the longer wavelengths was applied to Eq. (5). For computations, we employ the same Green's function approach as for the isostatic anomalies (Eq. (4)).

A sum of the isostatic anomalies and decompensative correction gives the decompensative gravity anomalies:

$$\Delta g_d = \Delta g_i + \Delta g_{dc} \tag{6}$$

2.2. Initial data

For the initial gravity anomalies, we employed the EIGEN-6C4 model (Förste et al., 2014), based on a combination of terrestrial and satellite data. The maximum resolution for EIGEN-6C4 is 2190 degree/order

(5'x5'), but the actual one locally depends on the available terrestrial and airborne data. However, even the resolution of the satellite only data (~70 km) is sufficient for the purposes of the present study. It is clear from Fig. 4a that the initial free air anomalies (disturbances) show much more local details for most of the CB and surrounding areas. For the topography we used the SRTM30_PLUS model (Becker et al., 2009), which was downscaled to the resolution 5'x5' corresponding to the initial gravity field (Fig. 2).

For calculation of the isostatic and decompensative gravity anomalies also information on the Moho position and EET is required. The map of the Moho from the model CRUST1.0 (Laske and Masters, 2013) and EET from Tesauro et al. (2012) are used in this study. The Moho map may have significant uncertainties, since it is not well constrained by seismic observations. However, this is not crucial in case of such large values of EET (>65 km for most of the study area). For example, for the very different crustal models CRUST2.0 (Laske et al., 2001) and CRUST1.0 (Laske and Masters, 2013), the difference of the isostatic corrections is less than ± 1 mGal. The EET has been determined on a global scale by two independent methods (geomechanical modeling and cross spectral analysis of the gravity field and topography), which provide similar values for the study area (Tesauro et al., 2012). Here we use the results of geomechanical modeling (Tesauro et al., 2012). The high values of EET are also close to those ones characterizing tectonically similar cratonic areas and fit in the range obtained by Kadima et al. (2011b). Although the employed EET map is in agreement with the results of different independent methods, some studies suggest that EET of the cratonic lithosphere is much less (20–40 km) (McKenzie and Fairhead, 1997). In particularly, McKenzie et al. (2014) obtained EET = 31–34 km for the Congo craton. We test this option when analysing the results.
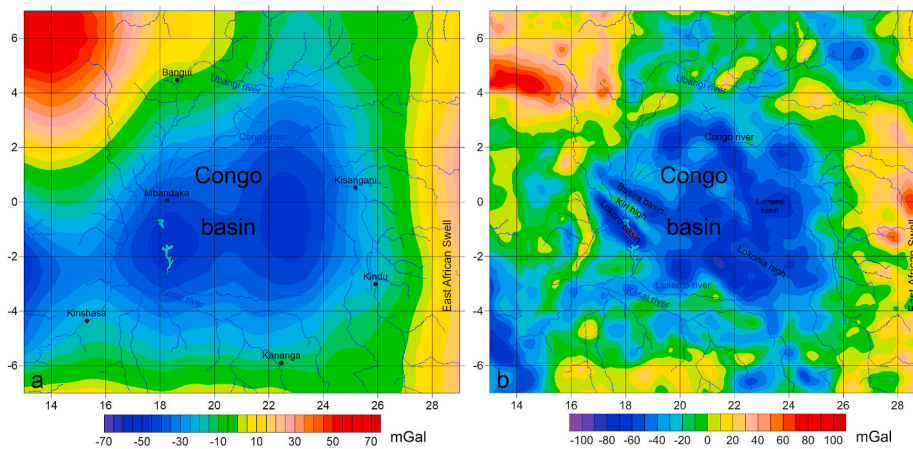
Fig. 6. Decompensative correction (a) and decompensative gravity anomalies (b).

2.3. Isostatic and decompensative gravity anomalies for the Congo basing and surrounding areas

The Bouguer gravity anomalies (Fig. 5a) have been computed by subtracting the effect of topography from the initial free air gravity (Fig. 4a). The calculation radius has been extended to 3° (333.6 km) compared to the usual 1.5°-2°. Numerical tests demonstrated that the topography variations outside this radius cause long-wavelength variations of the gravity field, which are not considered in this study. The anomalous effect of water in the adjacent areas is also included. The calculation method takes into account distribution of the topography elements on the sphere (Kaban et al., 2016). The Bouguer gravity anomalies, shown in Fig. 5a, are primarily dominated by the east-west trend reflecting general increase of the topography.

The isostatic correction is computed following Eq. (4) based on the adjusted topography (Fig. 2) extended by 1250 km in each direction to avoid boundary effects. Since compensating masses are located at some depth (primarily related to the Moho), the calculation radius should be increased compared to the calculation of the topography effect (Kaban, 2008). After applying the isostatic correction, the long-wavelength component (Fig. 5c, λ > 2500 km, half amplitude) has been removed from the isostatic anomalies as described above. This long-wavelength anomaly likely reflects the effect of mantle convection as suggested by previous authors (e.g., Crosby et al., 2010; Forte et al., 2010). The residual isostatic gravity anomalies are shown in Fig. 5b. As it was supposed, they are mostly dominated by small-scale variations over the CB, since the larger anomalies are likely reduced by the isostatic compensation as shown in Fig. 3. In order to recover the long-wavelength anomaly, we further apply the decompensative correction.

Based on the isostatic anomalies, we have computed the decompensative correction (Fig. 6a) using the Moho depth and EET shown in Fig. 4c–d. The amplitude of this field reaches ±70 mGal that even exceeds the amplitudes of the isostatic anomalies (Fig. 5b). Furthermore, the decompensative correction is dominated by long wavelengths, which is due to the high EET employed in the study area. The main negative pattern perfectly fits shape of the CB (Fig. 6a). This correction reflects the effect of positive density anomalies located at some depth under the CB, as was hypothesized earlier (e.g. Hartley and Allen, 1994). This finding also agrees with the results of geodynamic modelling of Downey and Gurnis (2009), who argued that the gravity anomaly and topography over the CB can be explained by the presence of dense material in the upper mantle likely associated with compositional changes. Alternatively, Crosby et al. (2010) suggested that the sub-Moho density anomaly could also be caused by mantle convection.

If we assume lower values of EET (31–34 km) as suggested by McKenzie et al. (2014), the decompensative correction will have more than double the amplitude, by more than 80 mGal larger in the Congo

Table 1

Average density of the main sedimentary sequences within the CB (Kadima et al., 2011a), g/cm³. The average depth range at which the density value is provided, with the maximum depth values under brackets from Maddaloni et al. (2019).

Seismic Unit	Age	Lithology	Depth-range (m)	Average density
C	Jurassic-Cenozoic	Sandstones, siltstones	0-1000 (1500)	2.25
B	Paleozoic-Triassic	Sandstones, glacial tillites & shales	1000-2000 (3000)	2.45
A	Late Mesoproterozoic-Neoproterozoic	Clastics, shales, (dolomitic) limestone, minor salt & anhydrite	2000-5000 (9000)	2.55
Crystalline basement	Precambrian	Granites & gneiss	5000–9000	2.7

Basin. Therefore, the decompensative anomalies would exceed −200 mGal in the central part of the Congo basin, whose value cannot be explained by any plausible density-depth relation even for a very deep basin (see below). Therefore, we conclude that the high EET is more appropriate for the Congo craton.

The resulting decompensative gravity anomalies are shown in Fig. 6b. Most of the CB is characterized by negative anomalies. The amplitude of the negative anomalies reaches −100 mGal, which agrees with the results of direct modeling of the gravity effect of sediments for North America and Eurasia (Kaban and Mooney, 2001; Mooney and Kaban, 2010; Kaban et al., 2016b). The field is well structured and distinguished anomalies should correspond to sub-basins and regional highs, which is discussed in the next chapter.

3. Discussion

Sediments are the main factor responsible for the negative decompensative gravity anomalies, however they depend on both, density and thickness of the sedimentary layer (Haeger and Kaban, 2019). Therefore, for estimation of sedimentary thickness from the decompensative gravity anomalies, it is necessary to know density distribution within the sedimentary body. Unfortunately, there exist very limited data on density of sediments, which are summarized in Kadima et al. (2011a) and shown in Table 1. The CB sediments are composed of several layers, which are displayed in Table 1 together with the densities estimated for each of them from Compensated Neutron Density Logs and from sample measurements (Kadima et al., 2011a). It should be noted that these
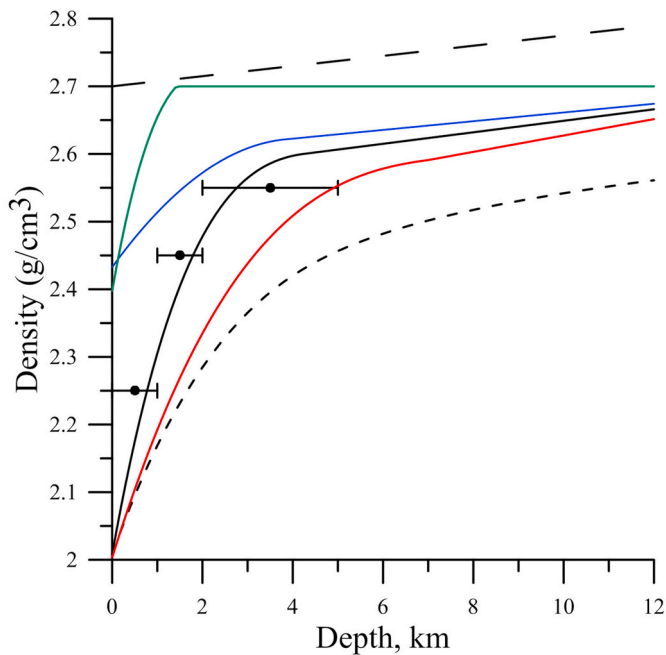
Fig. 7. Density depth relationship curves. Black curve represents the density-depth relationship used in this study, based on compaction curves, obtained from Mooney and Kaban (2010). Horizontal bars show density ranges from Table 1 (Kadima et al., 2011a). Short-dash curve is the vertically averaged density (related to the total gravity effect). Long-dash line is the reference density for the crystalline crust according to Christensen and Mooney (1995). For comparison, several other curves representing continental-type relationships for different basins from Mooney and Kaban (2010) are displayed: (Red) Gulf of Mexico; (Blue) most of intracontinental foredeeps; (Green) very dense Michigan and Illinois basins.

Fig. 8. Thickness of sediments obtained from the inversion of the negative decompensative gravity anomalies with the predefined density-depth relationship. Thick black lines show seismic profiles (Delvaux et al., 2021), which are displayed in Fig. 9.

density determinations are preliminary at this stage and characterize relatively shallow horizons since the maximum depth of the existing wells is about 4.3–4.5 km (2 wells), while others only reach the depth ~2 km.

Available seismic reflection profiles allow the reconstruction of the stratigraphy only in some parts of the CB (in the Democratic Republic of the Congo, south of the Congo River), since industrial studies (in the Republic of Congo, north of the Congo River) remain unpublished. This makes it difficult to construct a general stratigraphic model for the whole basin. Jachens and Moring (1990), when studying thickness of sediments in Nevada, suggested a reasonable approach to use a generalized density-depth relation, which is constructed for specific types of sediments based on depth-compaction curves. In this way it is possible to study regional variations of sedimentary structure while ignoring local anomalies. This approach was successfully used in many studies of sedimentary basins of several continents, as for those of North America (e.g. Mooney and Kaban, 2010), Eurasia (e.g. Kaban et al., 2016b), and Antarctica (Haeger and Kaban, 2019). Here, we follow this approach for determination of the sedimentary thickness in the CB.

The depth ranges and density for specific sedimentary layers from Table 1 are shown in Fig. 7 (Kadima et al., 2011a). Indeed, they represent a clear trend when the density increases with depth. Mooney and Kaban (2010) analysed possible density-depth relationships for various kinds of continental basins. The only one (black line, Fig. 7), which is based on a pure compaction curve (0–4.5 km), fits to the density-depth ranges displayed in Table 1. Below 4.5 km, this curve represents just linear interpolation to the maximum density 2.7 g/cm³ at the depth 15 km (Mooney and Kaban, 2010). All other curves are located out of the specified density-depth ranges (Fig. 7). Therefore, the black curve was used in this study.

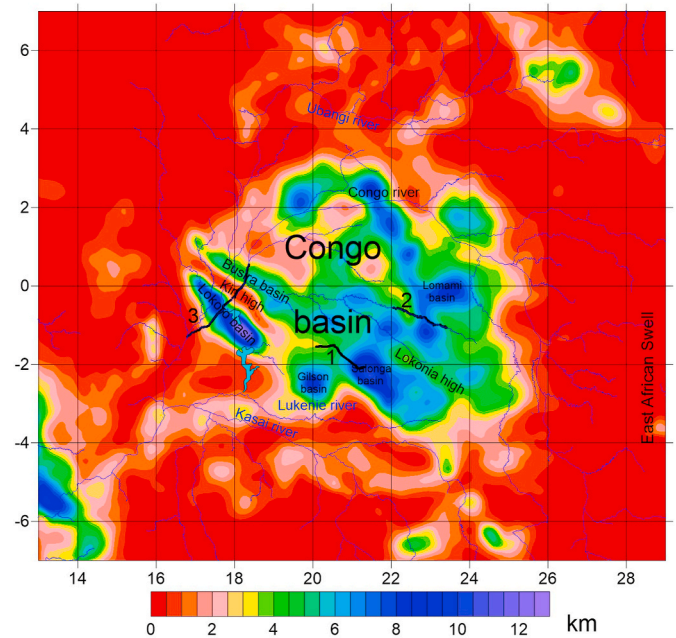The employed density-depth relationship is just a first approximation

and the results are rather qualitative than quantitative, showing chiefly relative variations of the sedimentary thickness. For example, a significant uncertainty could result from the very dense layer of the dolomitic carbonates, whose density is close to the density of the surrounding crystalline crust. However, thickness of this layer is small (<1.5 km, Kadima et al., 2011a). The vertically averaged density for the whole column, which directly relates to the total gravity effect, is also displayed in Fig. 7. This curve and that representing the density-depth relationship more consistent with the average density values (Table 1) were used to estimate sedimentary thickness from the decompensative anomalies. The density difference from the surrounding crystalline crust was determined relative to a linear trend starting from 2.7 g/cm³ at the surface through 2.76 g/cm³ at 8 km. This trend is estimated according to the statistical analysis of seismic data for continental platforms (Christensen and Mooney, 1995).

The inversion for sedimentary thickness was done in an iterative procedure. In the first step, the thickness has been determined as for the simple Bouguer correction by fitting the equation:

$$\Delta g_d = 2\pi G\, S\, \left(\overline{\rho}_S(S) - \overline{\rho}_{ref}(S) \right), \tag{7}$$

where S is the thickness of sediments, $\overline{\rho}_S(S)$ is the average density of sediments, and $\overline{\rho}_{ref}(S)$ is the average reference density of the crystalline crust. In practice, we have plotted the right-hand term and determined the thickness S, which fits to the negative decompensative anomaly in each point. In the next step, the gravity effect of sediments has been estimated for the determined thickness by using a 3D algorithm on the sphere (Kaban et al., 2016). The difference with the original decompensative anomalies was used then to estimate corrections for the initial sedimentary thickness. The convergence is reached very fast since 3D effects are not significant for small depths.

The sedimentary thickness map obtained by inversion of the negative decompensative gravity anomalies with the predefined density-depth relationship is displayed in Fig. 8. We can observe that the maximum depth of the obtained sedimentary layer exceeds 10 km. However, we should consider the possible uncertainties of the calculated values,
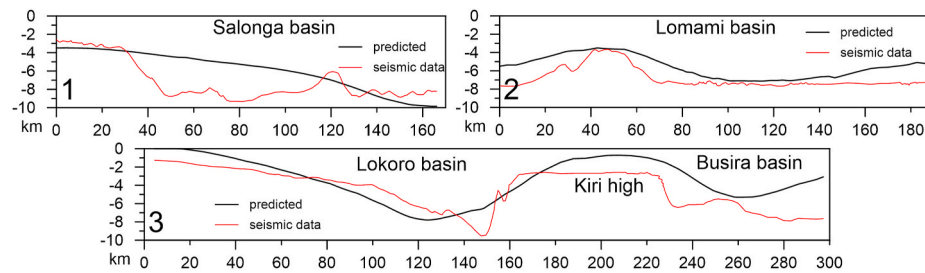
Fig. 9. Comparison of the predicted thickness of sediments with seismic determinations (Delvaux et al., 2021). Locations of the profiles are shown in Fig. 8.

which progressively increase with depth, due to flattening of the density-depth relationship. If we follow Mooney and Kaban (2010) and assume that the typical density uncertainty is about 15%, possible deviations for the thickness 2 km would be 1.55–2.6 km and for the thickness 4 km– 2.9–5.35 km. Then, after approximately 7.5 km, the upper limit becomes undefined even if we assume that the total uncertainty of the average density is less than of a single layer. Therefore, for the depths larger than 7 km, the thickness estimations are rather qualitative. Also, as explained before, it is hardly possible to define the exact depth of the basement, since the density contrast with the surrounding crust is small. The obtained values of the sedimentary thickness have been compared with available seismic profiles (Delvaux et al., 2021). This comparison shows that the agreement between the observed and predicted values is even better than stated above. For the depth range 0–3 km, RMS of the difference between them is equal to 1.62 km, therefore on the lower limit of the prediction. For the interval 3–6 km, the RMS is equal to 2.21; and for the depths exceeding 6 km, it is equal to 4.03 km. The last value chiefly reflects underestimation of the thickness of very deep basins as expected above. These values can be considered as a proxy of determination uncertainties.

In Fig. 9, we display seismic profiles for three key regions (Delvaux et al., 2021) showing thickness of sediments compared with the predicted values. It is clear that main features are reliably reproduced by the gravity field analysis. The main differences are related to small scale details. This is expectable, since the resolution of the gravity field is chiefly determined by the satellite data, whose resolution doesn't exceed 70 km (Förste et al., 2014). In this way, the predicted thickness of sediments doesn't reproduce the sharp change at the border of the Salonga basin (Profile 1, Fig. 9), although the maximal and minimal values of thickness on both sides are correct. The same is true for the Lomami basin (Profile 2, Fig. 9) and for the Lokoro and Busira basins divided by the Kiri High (Profile 3, Fig. 9). The differences of the observed and predicted values correspond to the above estimates, e.g. the maximal value is observed for the very deep part of the transition to the Salonga basin (Profile 1, Fig. 9). In most other places this difference does not exceed 2.3 km.

The largest sedimentary thickness is reached in the parts of the Congo basin, such as the Lokoro basin, Gilson basin, and the Lomami basin in the north (Fig. 8). It is worth noting that some of the deepest sub-basins, as those located north to the Lomami basin, are not identified by seismic studies, which only partly cover the central part of the Cuvette Central.

The obtained sediments' thickness map clearly shows the continuity of the tectonic structures, which are partially observed by the seismic profiles (Kadima et al., 2011a). Those are located in the southern and central parts and have been shot to highlight the structure of the basin, which was expected from the integration of aeromagnetic and gravity data, refraction seismics, and the 4 stratigraphic and exploration wells (Cahen et al., 1959, 1960; Jones et al., 1960; JNOC, 1984; ECL, 1988; Kadima et al., 2011a, b). However, the seismic reflection profiles are widely spaced and do not allow alone to demonstrate the lateral extension of the structures observed. The structure of the basin obtained in this study is consistent with the first-order interpretation from the

industry reports (ECL) and earlier publications (Lawrence and Makazu, 1988). However, the basement deep adjacent to the Lokonia High (on the SW side) was not known before. It is therefore a new structure that we propose to name as the Salonga basin, from the name of the river and of the national park and UNESCO World Heritage Centre just above it. This basin appears as the deepest of the entire Congo Basin. It has been overlooked because of the poor resolution of the seismic profile, which runs partly through it. It is worth pointing that the Salonga Basin is also visible in the initial free air anomalies (Fig. 4a), which supports that this structure is robust to some errors and ambiguities in the modelling.

Several sedimentary structures having a circular shape (e.g., Gilson basin) or elongated in NW-SE direction (e.g., Lokoro and Busira basin) are in a general agreement with the tectonic patterns of the CB, showing the Precambrian rift oriented in the same direction (e.g., Kadima et al., 2011b). The Lokoro and Busira basins are divided by the Kiri high, where the thickness of sediments is reduced, as well as by the Lokonia high, which forms a continuous NNW-SSE oriented structure dividing the Salonga basin in the south from the sedimentary sub-basins in the northern part.

4. Conclusions

Here, we present estimations of the sedimentary thickness in the whole CB, based on the analysis of the decompensative gravity anomalies. Usually, Bouguer or isostatic gravity anomalies are widely used to identify shallow crustal structures, such as sedimentary basins. However the effect of sediments in these anomalies is significantly reduced by deep compensating masses. To recover this effect, we estimate the decompensative correction, which reaches ±70 mGal over the CB, exceeding the amplitude of the initial isostatic anomalies. Using this correction and the isostatic anomalies we obtained the decompensative gravity anomalies, whose pattern perfectly fits to the shape of the CB and reveals tectonic fragmentation of this structure.

By inverting the decompensative gravity anomalies with the predefined density-depth relationship we have obtained the sedimentary thickness map for the whole CB. The maximum basement depth, exceeding 10 km, is found in the Lokoro and Salonga basins, while in the Lomami basin, thickness of sediments reaches about 6.5 km. This confirms the earlier results from unpublished industry reports except for the Salonga deep, which was previously unknown.

This study for the first time gives a general view on the distribution of the sedimentary thickness in the whole CB. Despite these estimates for the deepest parts are rather qualitative than quantitative, they provide a background for planning future studies.

Declaration of competing interest

The authors declare that they have no known competing financial interests or personal relationships that could have appeared to influence the work reported in this paper.

Acknowledgments

References

Ayele, A., 2002. Active compressional tectonics in Central Africa and implications for plate tectonic models: evidence from fault mechanism studies of the 1998 earthquakes in the Congo Basin. J. Afr. Earth Sci. 35, 45–50.

Becker, J.J., Sandwell, D.T., Smith, W.H.F., Braud, J., Binder, B., Depner, J., et al., 2009. Global bathymetry and elevation data at 30 arc seconds resolution: SRTM30_PLUS. Mar. Geodes. 32 (4), 355–371.

Blakely, R.J., 1995. Potential Theory in Gravity and Magnetic Applications. Cambridge University Press, London, p. 464. Jan 27, Science.

Braitenberg, C., Ebbing, J., Götze, H.J., 2002. Inverse modelling of elastic thickness by convolution method–the Eastern Alps as a case example. Earth. Planet. Sci. Letts. 202 (2), 387–404.

Buiter, S.J.H., Steinberger, B., Medvedev, S., Tetreault, J.L., 2012. Could the mantle have caused subsidence of the Congo Basin? Tectonophysics 514–517, 62–80.

Burke, K., Gunnell, Y., 2008. The African erosion surface: a continental-scale synthesis of geomorphology, tectonics, and environmental change over the past 180 million years. Geol. Soc. Am. Mem. 201. https://doi.org/10.1130/2008.1201.

Cahen, L., Ferrand, J.J., Haarsma, M.J.F., Lepersonne, J., Vebeek, Th, 1959. Description du Sondage de Samba. Ann. Mus. Roy. Congo belge, Tervuren (Belgique), série in-8. Sci. Geol. 29, 210pp.

Cahen, L., Ferrand, J.J., Haarsma, M.J.F., Lepersonne, J., Vebeek, Th, 1960. Description du Sondage de Dekese. Ann. Mus. Roy. Congo belge,Tervuren (Belgique), série in-8. Sci. Geol. 34, 115pp.

Christensen, N.I., Mooney, W.D., 1995. Seismic velocity structure and composition of the continental crust: a global review. J. Geophys. Res. 100, 9761–9788.

Cordell, L., Zorin, Y.A., Keller, G.R., 1991. The decompensative gravity anomaly and deep structure of the region of the Rio Grande rift. J. Geophys. Res.: Solid Earth 96 (B4), 6557–6568.

Craig, T.J., Jackson, J.A., Priestley, K., McKenzie, D., 2011. Earthquake distribution patterns in Africa: their relationship to variations in lithospheric and geological structure, and their rheological implications. Geophys. J. Int. 185 (1), 403–434.

Crosby, A.G., Fishwick, S., White, N., 2010. Structure and evolution of the intracratonic Congo Basin. Geochem. Geophys. Geosyst. (G3) 11 (6), Q06010.

Daly, M.C., Lawrence, S.R., Kimun'a, D., Binga, M., 1991. LatePaleozoic deformation in central Africa: a result of distant collision? Nature 350, 605–607.

Daly, M.C., Lawrence, S.R., Diemu Tshiband, K., Matouana, B., 1992. Tectonic evolution of the Cuvette Centrale, Zaire. J. Geol. Soc. London 149, 539–546.

De Wit, M.J., Stankiewicz, J., Reeves, C.V., 2008. Restoring Pan-African-Brasiliano Connections: More Gondwana Control, Less Trans-Atlantic Corruption. Geological Society, London, Special Publications, vol. 294. https://doi.org/10.1144/SP294.20.

Delvaux, D., Barth, A., 2010. African stress pattern from formal inversion of focal mechanism data. Tectonophysics 482, 105–128. https://doi.org/10.1016/j.tecto.2009.05.009, 2010.

Delvaux, D., Maddaloni, F., Tesauro, M., Braitenberg, C., 2021. The Congo Basin: stratigraphy and subsurface structure defined by regional seismic reflection, refraction and well data. Global Planet. Change 198, 103407. https://doi.org/10.1016/j.gloplacha.2020.103407.

Dill, R., Klemann, V., Martinec, Z., Tesauro, M., 2015. Applying local Green's functions to study the influence of the crustal structure on hydrological loading displacements. J. Geodyn. 88, 14–22.

Downey, N.J., Gurnis, M., 2009. Instantaneous dynamics of the cratonic Congo basin. J. Geophys. Res. 114, B06401. https://doi.org/10.1029/2008JB006066.

Ebbing, J., Braitenberg, C., Wienecke, S., 2007. Insights into the lithospheric structure and the tectonic setting of the Barents Sea region from isostatic considerations. Geophys. J. Int. 171, 1390–1403. https://doi.org/10.1111/j.1365-246X.2007.03602.x.

ECL, 1988. Hydrocarbon Potential of Cuvette Centrale (Republic of Zaire). Exploration Consultants Limited, CelluleTechnique. Petrolière, Petrozaire, unpublished report, 41pp. figures, tables, appendices and enclosures.

Exxon Production Research Company, 1985. Tectonic Map of the World. American Association of Petroleum Geologists Foundation, Tulsa, OK, USA.

Fairhead, J.D., Stuart, G.W., 1982. Seismicity of the east Africa Rift System and comparison with other continental rifts. In: Palmason, G. (Ed.), Continental and Oceanic Rifts, Geodynamics Series, 8. American Geophysical Union, Washington, D. C., pp. 41–61. United States of America.

Förste, C., Bruinsma, S., Abrikosov, O., Flechtner, F., Marty, J.-C., Lemoine, J.-M., Marty, J., 2014. EIGEN-6C4 - the latest combined global gravity field model including GOCE data up to degree and order 1949 of GFZ Potsdam and GRGS Toulouse. EGU General Assembly 16, 3707. https://doi.org/10.5880/icgem.2015.1.

Forsyth, D.W., 1985. Subsurface loading and estimates of the flexural rigidity of continental lithosphere. J. Geophys. Res. Planets 90, 12623–12632. https://doi.org/10.1029/JB090iB14p12623.

Forte, A.M., Quéré, S., Moucha, R., Simmons, N.A., Grand, S.P., Mitrovica, J.X., Rowley, D.B., 2010. Joint seismic–geodynamic-mineral physical modelling of African geodynamics: a reconciliation of deep-mantle convection with surface geophysical constraints. Earth Planet Sci. Lett. 295 (3–4), 329–341.

Haeger, C., Kaban, M.K., 2019. Decompensative gravity anomalies reveal the structure of the upper crust of Antarctica. Pure Appl. Geophys. 1–14 https://doi.org/10.1007/s00024-019-02212-5.

Hartley, R., Allen, P.A., 1994. Interior cratonic basins of Africa: relation to continental breakup and role of mantle convection. Basin Res. 6, 95–113.

Hildenbrand, T.G., Griscom, A., Van Schmus, W.R., Stuart, W.D., 1996. Quantitative investigations of the Missouri gravity low: a possible expression of a large, Late Precambrian batholith intersecting the New Madrid seismic zone. J. Geophys. Res. Solid Earth 101 (B10), 21921–21942, 1978–2012.

Jachens, R.C., Moring, C., 1990. Maps of the thickness of Cenozoic deposits and the isostatic residual gravity over basement for Nevada. U.S. Geol. Surv. Open File Rep. 90–404, 15.

JNOC, 1984. Rapport des investigations géophysiques et géologiques dans la Cuvette centrale de la République du Zaïre. Japan National Oil Corporation, Report for Department of Mines and Energy, Government of Zaire, Unpublished, p. 205pp.

Jones, L., Mathieu, P.L., Strenger, H., 1960. Gravimétrie:Les résultats scientifiques des missions du syndicat pour l'étude géologique et minière de la Cuvette Congolaise et travaux connexes. Ann. Mus. Roy. Congo belge, Tervuren (Belgique), série in-8. Sci. Geol. 36, 46pp.

Kaban, M.K., Mooney, W.D., 2001. Density structure of the lithosphere in the Southwestern United States and its tectonic significance. J. Geophys. Res. 106 (B1), 721–740.

Kaban, M.K., Schwintzer, P., Tikhotsky, S.A., 1999. Global isostatic residual geoid and isostatic gravity anomalies. Geophys. J. Int. 136, 519–536.

Kaban, M.K., Schwintzer, P., Reigber, Ch, 2004. A new isostatic model of the lithosphere and gravity field. J. Geodes. 78, 368–385.

Kaban, M.K., El Khrepy, S., Al-Arifi, N., 2016. Isostatic model and isostatic gravity anomalies of the Arabian plate and surroundings. Pure Appl. Geophys. 173 (4), 1211–1221. https://doi.org/10.1007/s00024-015-1164-0.

Kaban, M.K., Stolk, W., Tesauro, M., El Khrepy, S., Al-Arifi, N., Beekman, F., Cloetingh, S. A.P.L., 2016b. 3D density model of the upper mantle of Asia based on inversion of gravity and seismic tomography data. Geochem. *Geophys. Geosyst.* 17 https://doi.org/10.1002/2016GC006458.

Kaban, M.K., El Khrepy, S., Al-Arifi, N., 2017. Importance of the decompensative correction of the gravity field for study of the upper crust: application to the Arabian plate and surroundings. Pure Appl. Geophys. 174 (1), 349–358.

Kadima, E., Delvaux, D., Sebagenzi, S.N., Tack, L., Kabeya, S.M., 2011a. Structure and geological history of the Congo Basin: an integrated interpretation of gravity, magnetic and reflection seismic data. Basin Res. 23 (5), 499–527.

Kadima, E., Sebagenzi, S.N., Lucazeau, F., 2011b. A Proterozoic-rift origin for the structure and the evolution of the cratonic Congo basin. Earth Planet Sci. Lett. 304, 240–250.

Langenheim, V.E., Jachens, R.C., 1996. Gravity data collected along the Los Angeles regional seismic experiment (LARSE) and preliminary model of regional density variations in basement rocks, southern California. U.S. Geol. Surv. Open File Rep. 96–682, 25.

Laske, G., Masters, G., 2013. Update on CRUST1.0 —a 1-degree global model of Earth's crust. Geophys. Res. Abstr. 15, EGU2013–2658.

Laske, G., Masters, G., Reif, C., 2001. CRUST2. 0: a new global crustal model at 2× 2 degrees. Institute of Geophysics and planetary physics, the University of California, san Diego, website. http://mahi.ucsd.edu/Gabi/rem.dir/crust/crust2.html.

Lawrence, S., Makazu, M.M., 1988. Zaire's Central basin: prospectivity outlook. Oil Gas J. 86 (38), 105–108.

Macgregor, D., 2015. History of the development of the East African Rift System: a series of interpreted maps through time. J. Afr. Earth Sci. 101, 232–252.

Maddaloni, F., Delvaux, D., Munch, J., Tesauro, M., Gerya, T., Braitenberg, C., 2019. Reconstruction of the sedimentary structure and subsidence of the Congo Basin using geophysical data and numerical models. Geophys. Res. Abstr. 21, EGU2019–5396.

McKenzie, D., Fairhead, D., 1997. Estimates of the effective elastic thickness of the continental lithosphere from Bouguer and free air gravity anomalies. J. Geophys. Res.: Solid Earth 102 (B12), 27523–27552.

McKenzie, D., Yi, W., Rummel, R., 2014. Estimates of Te from GOCE data. Earth Planet Sci. Lett. 399, 116–127.

Mooney, W.D., Kaban, M.K., 2010. the north American upper mantle: density, composition, and evolution. J. Geophys. Res. 115, B12424. https://doi.org/10.1029/2010JB000866.

Pivetta, T., Braitenberg, C., 2020. Sensitivity of gravity and topography regressions to earth and planetary structures. Tectonophysics 774, 228299. https://doi.org/10.1016/j.tecto.2019.228299.

Simpson, R.W., Jachens, R.C., Blakely, R.J., Saltus, R.W., 1986. A new isostatic residual gravity map of the conterminous United States with a discussion on the significance of isostatic residual anomalies. J. Geophys. Res. 91, 8348–8372, 1986.

Storchak, D.A., Di Giacomo, D., Bondár, I., Engdahl, E.R., Harris, J., Lee, W.H.K., Villaseñor, A., Bormann, P., 2013. Public release of the ISC-GEM global instrumental earthquake Catalogue (1900-2009). Seismol. Res. Lett. 84 (5), 810–815. https://doi.org/10.1785/0220130034.

Tesauro, M., Audet, P., Kaban, M.K., Bürgmann, R., Cloetingh, S., 2012. The effective elastic thickness of the continental lithosphere: comparison between rheological and inverse approaches. Geochem. Geophys. Geosyst. (G3) 13, Q09001.

Trouw, R.A.J., De Wit, M.J., 1999. Relation between the Gondwanide Orogen and contemporaneous intracratonic deformation. J. Afr. Earth Sci. 28 (1), 203–213.

Turcotte, D.L., Schubert, G., 1982. Geodynamics, second ed. Cambridge University Press, Cambridge, United Kingdom.

Watts, A.B., 2001. Isostasy and Flexure of the Lithosphere. Cambridge University Press, Cambridge ; New York.

Wienecke, S., Braitenberg, C., 2007. A new analytical solution estimating the flexural rigidity in the Central Andes. Geophys. J. Int. 789–794. https://doi.org/10.1111/j.1365-246X.2007.3396.x.

Wilson, D., Aster, R., West, M., Ni, J., Grand, S., Gao, W., Patel, P., 2005. Lithospheric structure of the Rio Grande rift. Nature 433 (7028), 851–855.

Zorin, Y.A., Pismenny, B.M., Novoselova, M.R., Turutanov, E.K., 1985. Decompensative gravity anomalies. Geologia i Geofizika 8, 104–108.

Zorin, Y.A., Belichenko, V.G., Turutanov, E.K., Kozhevnikov, V.M., Ruzhentsev, S.V., Dergunov, A.B., Khosbayar, P., 1993. The south Siberia-central Mongolia transect. Tectonophysics 225 (4), 361–378.

Kaban, M.K., 2008. Estimation of the effect of distant zones in gravity modeling of the lithosphere, 10. EGU General Assembly, Vienna, p. A-05174, 13–18 April 2008, Geophysical Research Abstracts.